

DETERMINATION OF THE LOOSENING COEFFICIENT AT LARGE SIZE WELDING NECK FLANGE JOINTS

András NAGY

Chemical and Food Engineering Department
Faculty of Mechanical Engineering
Technical University of Budapest
H-1521 Budapest, Hungary

Received: Aug. 15, 1994

Abstract

This paper deals with the calculation of gasket load drop caused by internal pressure at flange joints. The method published here makes possible to take into consideration the stiffness effect of the integrated part of the flange ring. The equations published refer to large size welding neck flanges but the method itself can be applied at any other types of flange joint, too. During the determination of the flange rotational stiffness the model shaped up by MURRAY and STUART [4] for calculating stress-state of welding neck flanges should have been made more precise. The preciseness of this method, as well as the convergence of trial-and-error calculations used were proved by results of calculations carried out on flange joint.

Keywords: pressure vessel, flange joint.

1. Introduction

Tests have proved that gasket load F_{T0} generated at seating condition in the flange joint presented in *Fig. 1* is decreasing on introduction of internal pressure. This fact may cause leakage in the case of unsatisfactory bolt pre-load. Therefore, in order to reach leak tightness the value of gasket load drop should be known so that the value of bolt pre-load could be determined by taking into consideration this effect. Models known from literature [2, 5, 6, 7] assume that the reduction of gasket load results from the elastic deformation of the joint. There were applied approximations in equations based on the above assumption to obtain closed formulae as a solution. As a result of these approximations the published equations do not take into consideration the real shape of the integrated part when determining flange stiffness. The above mentioned approximations especially at welding neck flanges used in the case of high-pressure cause error. This paper discusses a calculation method based on analytical equations making possible consideration of the above effect in a relatively simple way. The equations published refer to large diameter welding neck flanges at

pipelines and pressure vessels but the method itself can be applied at another types of flange joint, too. Results of calculations presented in Chapter 5 prove the preciseness of this calculation method.

2. Assumptions

Fig. 2 shows the loads acting on flange investigated as an element of flange joint under seating (a) and pressurized condition (b). As the figure shows, the pressure induced header end load F_P will change the system of internal loads in the flange so both the bolt and gasket loads are changing in accordance with *Eqs. (1) and (2)* comparing to ones at seating condition.

$$F_{CU} = F_{C0} + F_P - \Delta F_T, \quad (1)$$

$$F_{TU} = F_{T0} - \Delta F_T. \quad (2)$$

In order to determine the gasket load drop (ΔF_T) in the literature the loosening coefficient [5, 6, 7] was invented and it is defined by *Eq. (3)*. The loosening coefficient for a given engineering material and geometry as a structural characteristic was regarded and used as a constant.

$$D = \frac{\Delta F_T}{F_P} = \frac{K_C + 2 \cdot z_T \cdot z_P^* \cdot K}{K_C + K_T + 2 \cdot z_T^2 \cdot K}. \quad (3)$$

In the *Eq. (3)* K_C and K_T are the spring stiffness of bolts and gasket, while K is the rotational spring stiffness of the flange loaded by a couple. The z_P^* invented in the *Eq. (3)* is the virtual arm [6] used to substitute the equally distributed load generated by internal pressure for F_P header end load acting on z_P^* offset from bolt circle as *Fig. 3* shows. Further on a method will be presented allowing a more precise calculation model so that more precise prediction of the bolt pre-load needed to a given internal pressure can be obtained. In accordance with models presented in the literature [4, 5, 6] the flange rings at large diameter flange joints can be modelled as elastic ring so at the determination of flange stiffness the displacements of ring can be calculated from equations valid for elastic rings. In order to reduce the mistake coming from asymmetry of external and internal surfaces of tapered hub connected to flange ring, there was invented the so-called mean surface for reduction which bisects the wall thickness $\overline{AB'}$ (see *Fig. 4*) as well as it continues in the mean surface of the constant wall-thickness cylindrical shell symbolized by \overline{AB} and it is nominated as calculating surface [8]. During the solution, just as with MURRAY and STUART [4], the tapered hub was regarded as an axisymmetrically loaded

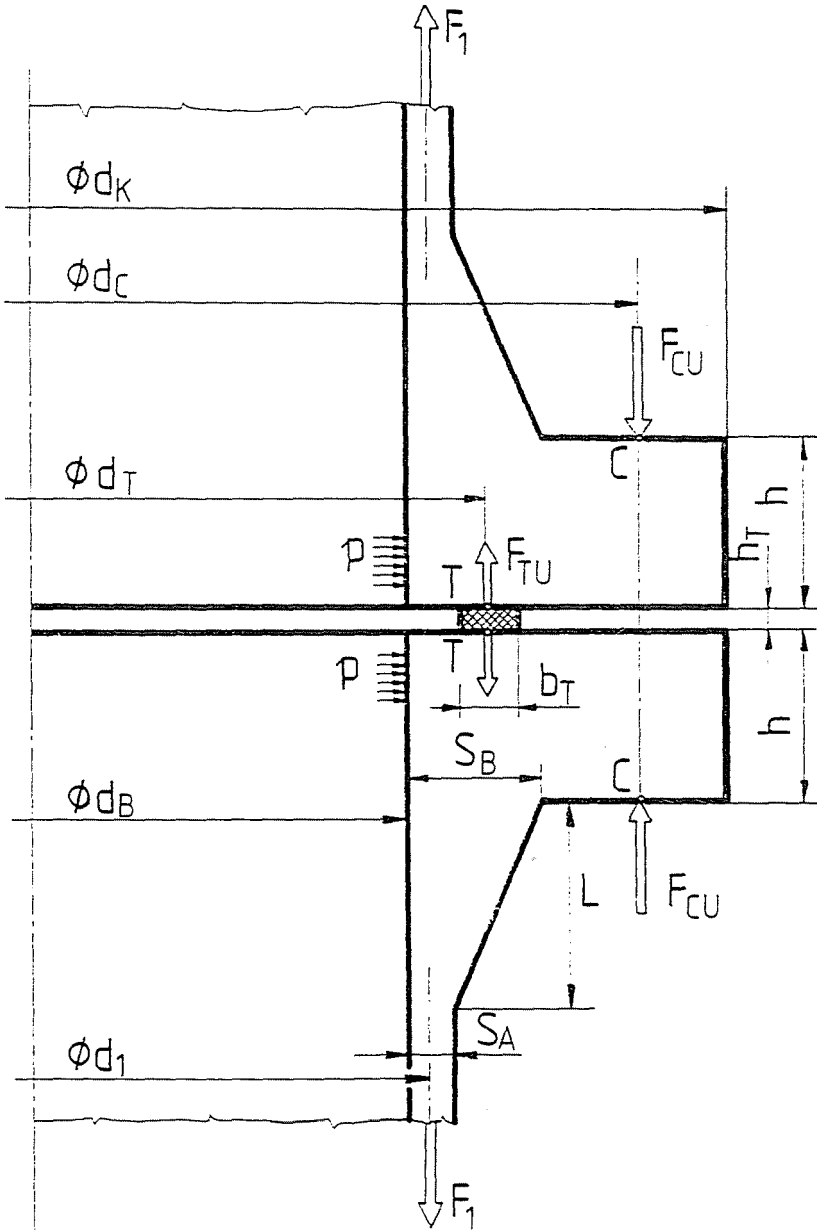


Fig. 1. Sketch of the investigated welded-neck flange joint

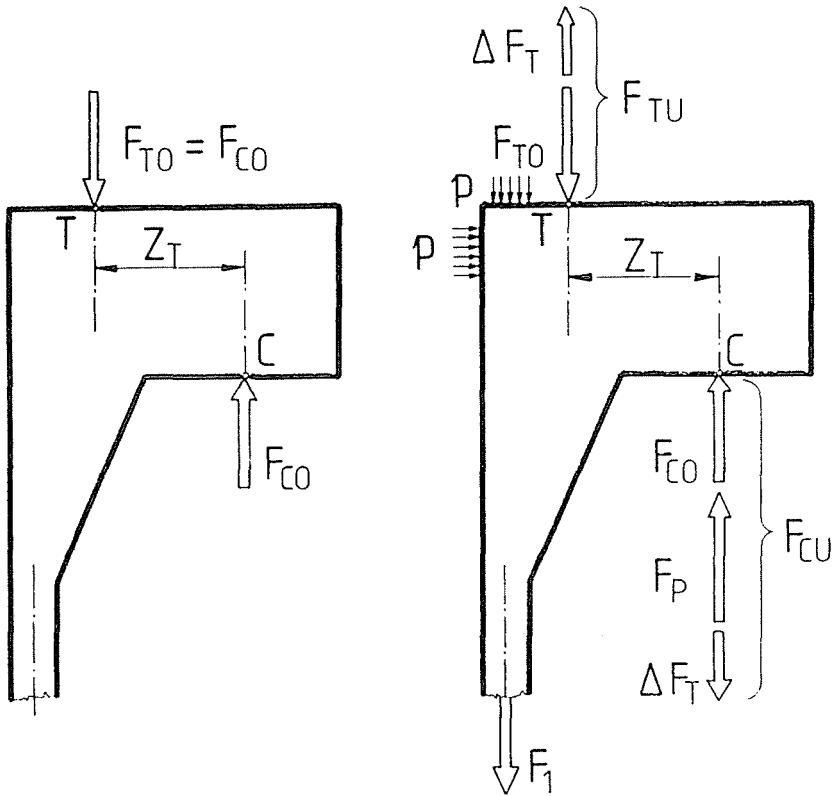


Fig. 2. The system of internal loads at seating and pressurized conditions

thin cylindrical shell with \overline{AB} mean surface having a linearly varying wall thickness. Then the edge forces and moments calculated as acting on the surface above were reduced on the true bisecting surface $\overline{AB'}$ of the tapered hub. The parameters arisen at the stiffness calculation of the integrated part of the flange ring were determined with variables given in Fig. 4 and a dimensionless coordinate expressed by Eq. (4)

$$\bar{x} = 5.264 \cdot (1 - \nu^2)^{0.25} \cdot d_1^{-0.5} \cdot \alpha^{-0.5} \cdot x^{0.5}, \quad (4)$$

where $\alpha = \operatorname{tg} \gamma$ and $\nu = 0.3$ the Poisson ratio of the flange material. The changes in effective gasket width caused by the deformation of flange ring were neglected at the model, that is the nominal width of the original geometry was taken into consideration in stiffness calculation. This approximate solution is acceptable at gaskets with high diameter and small width. In Chapter 3 assuming ideal elastic gasket material model but taking into

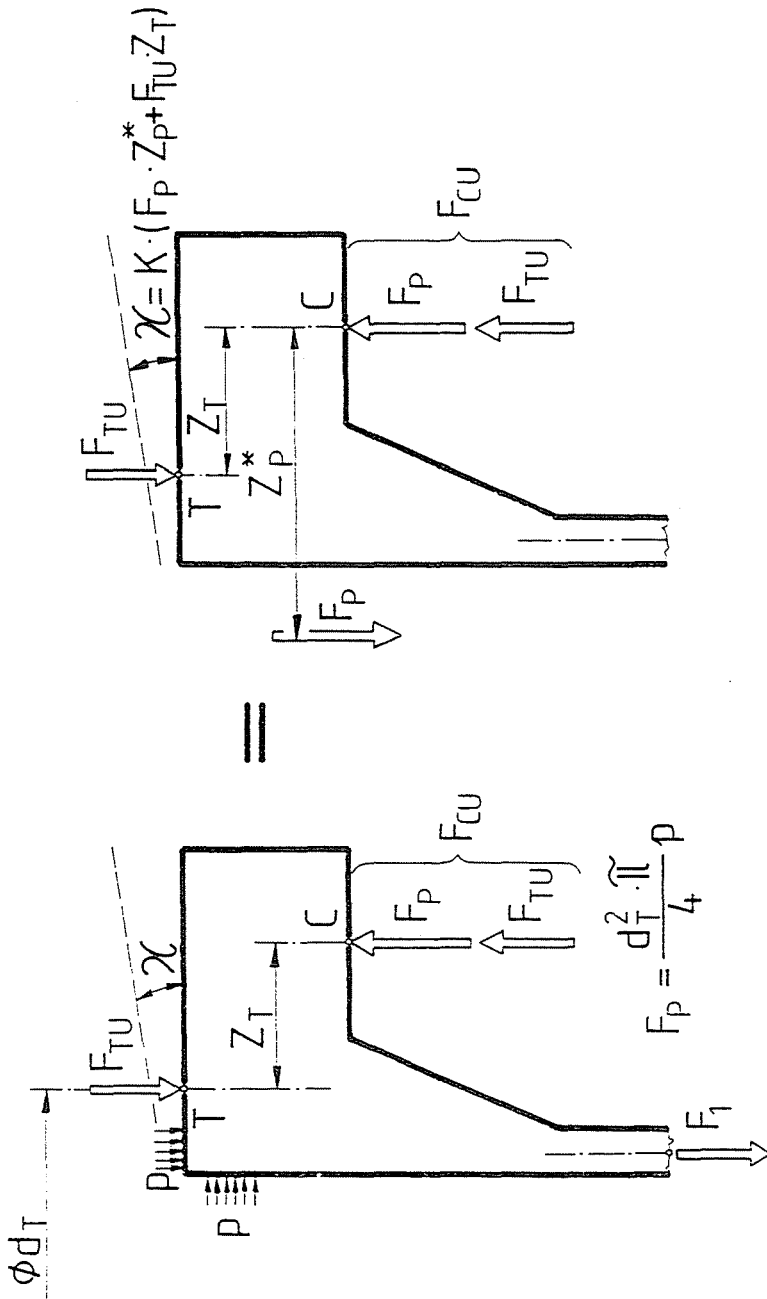


Fig. 3. Substitution of the distributed load for a couple

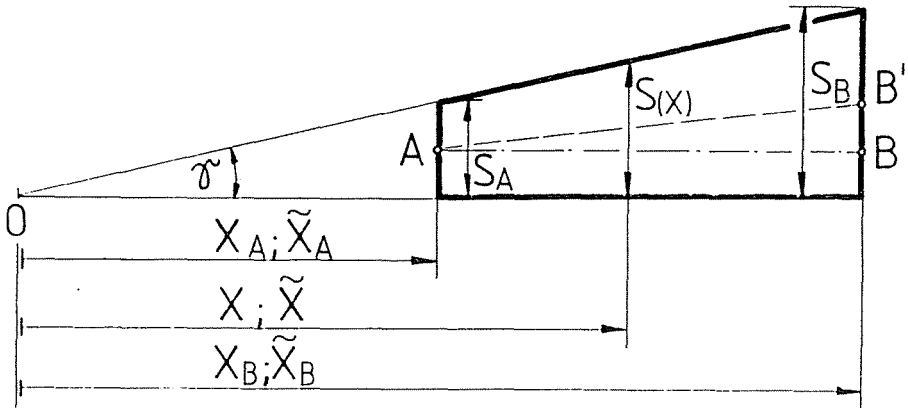


Fig. 4. Model of the tapered hub

consideration the effect of the integrated part of the flange ring, the loosening coefficient of the joint defined by Eq. (3) will be calculated. In Chapter 4 equations giving stress-state of integrated part of the flange-ring will be discussed. Finally, in Chapter 5 a numerical example presents the use of the published calculation model.

3. Loosening Coefficient of Flange Joint in the Case of Ideal Elastic Gasket Model

Fig. 5 represents the equilibrium of loads at flange ring and integrated part under seating (Fig. 5.a) and pressurized conditions (Fig. 5.b). Out of the system of loads acting on flange ring the meaning of F_{C0} and F_{CU} is bolt load under seating and pressurized condition while F_{T0} and F_{TU} are the gasket loads under seating and pressurized condition. Let us choose the required residual gasket load under pressurized condition $F_{TU} > F_{T\min}$ so the bolt pre-load under seating condition in accordance with Eqs. (1) and (2) can be calculated as:

$$F_{C0} = F_{T0} = D \cdot F_P + F_{TU}, \quad (5)$$

where $F_P = \left(\frac{d_T^2 \cdot \pi}{4} \right) \cdot p$ is the total header end load originated from internal pressure and D is the loosening coefficient of the joint. Among loads acting on flange ring the effect of integrated part can be expressed as shearing edge forces Q_{B0}, Q_{BU} and moments M_{B0}, M_{BU}, M_{F1} acting at the cross-section connected. The edge forces Q_{B0}, Q_{BU} and moments M_{B0}, M_{BU}

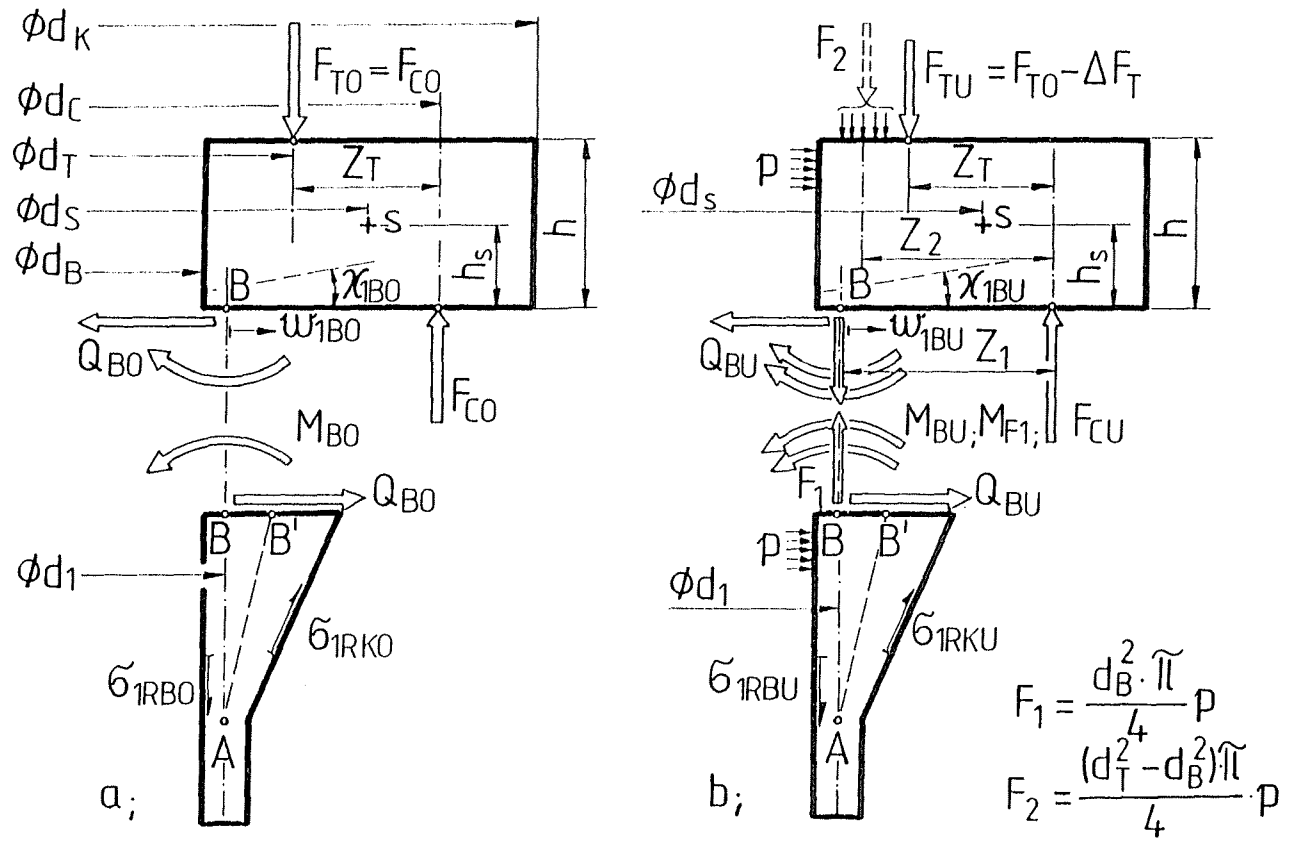


Fig. 3. Substitution of the distributed load for a couple

ensure the continuity of displacement as unknown parameters while edge moment M_{F_1} comes from the reduction of the axial load F_1 on surface \overline{AB} . Using the virtual arm of loads z_P^* (see *Fig. 3*) and the rotational spring stiffness of the flange K , the angular displacement of flange ring owing to internal pressure can be calculated as:

$$\Delta\chi = K \cdot (z_P^* \cdot F_P - z_T \cdot \Delta F_T). \quad (6)$$

In the case of large diameter flanges the flange ring can be regarded as an elastic ring so its angular displacement calculated according to *Eq. (6)* can also be given by using *Fig. 5* with *Eqs. (7, 8)*:

$$\Delta\chi = \chi_{1BU} - \chi_{1B0} = [F_1 z_1 + F_2 z_2 - \Delta F_T z_T - d_1 \pi (\Delta M_B + h_s \Delta Q_B)] \frac{d_s}{4\pi I E}, \quad (7)$$

where

$$\Delta M_B = M_{BU} + M_{F_1} - M_{B0}, \quad (8.a)$$

$$\Delta Q_B = Q_{BU} - Q_{B0}, \quad (8.b)$$

further on I means the moment of inertia of flange ring cross-section about the radial axis of symmetry while E means the modulus of elasticity of the flange material.

Using *Eqs. (6)* and *(7)*, the rotational stiffness of the flange and the virtual arm of loads can be obtained from the following equations:

$$K = \frac{d_s}{4\pi E I}, \quad (9)$$

$$z_P^* = \frac{F_1 z_1 + F_2 z_2}{F_P} - d_1 \pi \frac{(\Delta M_B + h_s \Delta Q_B)}{F_P}. \quad (10)$$

It can be stated on the basis of *Eqs. (9)* and *(10)* that in the expression of the loosening coefficient defined by *Eq. (3)* the effect of integrated part is expressed only by the virtual arm of loads z_P^* . In accordance with *Eq. (10)* to determine the virtual arm of loads z_P^* the internal edge forces and moments acting at the connection of flange ring should be known. These unknown internal forces and moments can be obtained from the following

Eqs. (11) and (12) representing the continuity of displacements in the connected cross-section as Fig. 5 shows.

$$w_{1B0} = M_{B0}\bar{w}_{MB} + Q_{B0}\bar{w}_{QB}, \quad (11.a)$$

$$\chi_{1B0} = M_{B0}\bar{\chi}_{MB} + Q_{B0}\bar{\chi}_{QB}, \quad (11.b)$$

$$w_{1BU} = M_{BU}\bar{w}_{MB} + Q_{BU}\bar{w}_{QB} + p\bar{w}_P, \quad (12.a)$$

$$\chi_{1BU} = M_{BU}\bar{\chi}_{MB} + Q_{BU}\bar{\chi}_{QB} + p\bar{\chi}_P. \quad (12.b)$$

The parameters defined in Eqs. (11) and (12) are: w_{1B0} and w_{1BU} the radial displacements of point B of the flange ring, while χ_{1B0} and χ_{1BU} the angular displacements at the connecting cross-section. These displacements as a function of forces and moments acting on flange ring can be calculated from equations given below:

$$w_{1B0} = \frac{M_{S0}d_S^2}{4IE}h_S + \frac{Q_{S0}d_Sd_1}{4AE}, \quad (13.a)$$

$$\chi_{1B0} = \frac{M_{S0}d_S^2}{4IE}, \quad (13.b)$$

$$w_{1BU} = \frac{M_{SU}d_S^2}{4IE}h_S + \frac{Q_{SU}d_Sd_1}{4AE}, \quad (14.a)$$

$$\chi_{1BU} = \frac{M_{SU}d_S^2}{4IE}. \quad (14.b)$$

where Q_{S0} , Q_{SU} , M_{S0} , M_{SU} represent the forces and moments distributed over unit length of circumference at the centre of gravity of the flange ring cross-section and they were calculated using the Eq. (15) and (16) under seating (Fig. 5.a) and pressurized condition (Fig. 5.b). That is:

$$Q_{S0} = -Q_{B0} \left(\frac{d_1}{d_S} \right), \quad (15.a)$$

$$M_{S0} = \frac{F_{C0zT}}{d_S\pi} - Q_{B0}h_S \left(\frac{d_1}{d_S} \right) - M_{B0} \left(\frac{d_1}{d_S} \right), \quad (15.b)$$

$$Q_{SU} = ph \left(\frac{d_B}{d_S} \right) - Q_{BU} \left(\frac{d_1}{d_S} \right), \quad (16.a)$$

$$M_{S\ddot{U}} = \frac{F_1 z_1 + F_2 z_2 + F_{TU} z_T}{d_S \pi} - Q_{BU} h_S \left(\frac{d_1}{d_S} \right) - (M_{BU} + M_{F1}) \left(\frac{d_1}{d_S} \right), \quad (16.b)$$

further on: I means the moment of inertia of flange ring cross-section (as it was used previously) and A means the area of the flange ring cross-section while, E stands for the modulus of elasticity of the engineering material. The \bar{w}_β and $\bar{\chi}_\beta$, where $\beta = (MB, QB, P)$ parameters appearing in Eqs. (11) and (12) mean the radial and angular displacements of the integrated part. The radial and angular displacements caused by the unit bending edge moment $\bar{w}_{MB}, \bar{\chi}_{MB}$ (see Fig. 6.a), by the unit shearing edge force $\bar{w}_{QB}, \bar{\chi}_{QB}$ (see Fig. 6.b) and by the unit internal pressure $\bar{w}_P, \bar{\chi}_P$ (see Fig. 6.c) can be calculated with equations below:

$$\bar{w}_\beta = e_1 \bar{c}_{j\beta} \psi'_j(\tilde{x}_B) + e_2 \quad (17.a)$$

$$\bar{\chi}_\beta = e_3 [\bar{c}_{(2i+1)\beta} \psi_{(2i+2)}(\tilde{x}_B) - \bar{c}_{(2i+2)\beta} \psi_{(2i+1)}(\tilde{x}_B)] - e_4 \bar{c}_{j\beta} \psi'_j(\tilde{x}_B) - e_5, \quad (17.b)$$

where $i = (0, 1)$; $j = (1, \dots, 4)$; $\beta = (MB, QB, P)$ further:

$$e_1 = x_B^{-0.5}. \quad (18.a)$$

In the case of $\beta = MB$ or $\beta = QB$ $e_2 = 0$, if $\beta = P$ then:

$$e_2 = 0.125 E^{-1} (2 - \nu) \alpha^{-1} [d_1 + \alpha(x_B - x_A)]^2 x_B^{-1}. \quad (18.b)$$

$$e_3 = 2.632 (1 - \nu^2)^{0.25} \alpha^{-0.5} d_1^{-0.5} x_B^{-1}, \quad (18.c)$$

$$e_4 = x_B^{-1.5}. \quad (18.d)$$

In the case of $\beta = MB$ or $\beta = QB$ $e_5 = 0$, if $\beta = P$ then:

$$e_5 = 0.125 E^{-1} (2 - \nu) \alpha^{-1} d_1^2 x_B^{-2}. \quad (18.e)$$

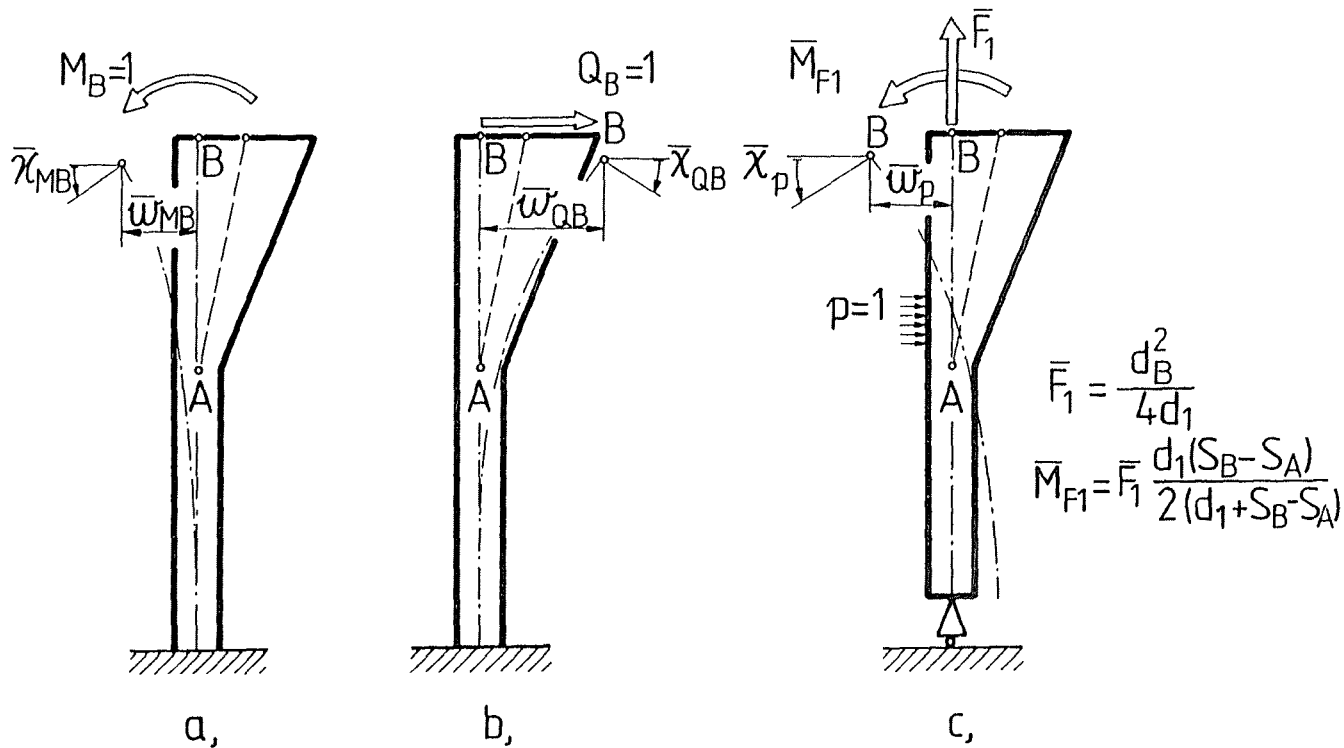


Fig. 6. The rotational and radial stiffness of the integrated part in case of uniform bending moment (a), shearing force (b) and internal pressure (c)

Table 1
The values of $b_{\beta i}$ appearing in Eq. (19)

β	i	$b_{\beta i}$
MB	1	1
	2	0
	3	0
	4	0
QB	1	0
	2	1
	3	0
	4	0
P	1	$\overline{M}_{F1} + \frac{0.02(2-\nu)\alpha^2 d_1^2}{1-\nu^2}$
	2	0
	3	$\frac{0.036(2-\nu)d_1^3}{E(1-\nu^2)^{0.5}x_A^2}$
	4	$\frac{(2-\nu)d_1^2}{E\alpha^{0.5}x_A^2} \left[\frac{0.134d_1}{(1-\nu^2)^{0.25}x_A^{0.5}} + \frac{0.125}{\alpha^{0.8}} \right]$

The ψ_j and $\psi'_j = \frac{d\psi_j}{dx}$ assign the Schleicher functions and their derivatives. The $\bar{c}_{j\beta}$ constants appearing in Eqs. (17.a) and (17.b) can be calculated by solving the boundary conditions equations below:

$$b_{\beta i} = a_{ij}\bar{c}_{j\beta}, \quad (19)$$

where $(i, j) = (1, \dots, 4)$.

The values for $b_{\beta i}$ used in Eq. (19) can be taken from Table 1, while coefficients a_{ij} can be calculated as a linear combination of Schleicher functions (20.a) and (20.b). In the case $i = (1, 2)$

$$a_{ij} = \eta_{ijk}\phi_k(\tilde{x}_B) \quad j = (1, \dots, 4), \quad k = (1, \dots, 8). \quad (20.a)$$

In the case $i = (3, 4)$:

$$a_{ij} = \eta_{ijk}\phi_k(\tilde{x}_A) \quad j = (1, \dots, 4), \quad k = (1, \dots, 8), \quad (20.b)$$

where non zero elements of η_{ijk} can be seen in Table 2, further $[\phi_1, \dots, \phi_8] = [\psi_1, \dots, \psi_4, \psi'_1, \dots, \psi'_4]$. In accordance with Eq. (5) on the connected cross-section of the flange ring at seating condition the shearing force Q_{B0} and

Table 2
The non-zero elements of η_{ijk} used in Eq. (20)

$\eta_{112} = -\eta_{121} = \eta_{134} = -\eta_{143} = 0.438E(1 - \nu^2)^{-0.75}\alpha^{2.5}d_1^{-0.5}x_B$
$-\eta_{115} = -\eta_{126} = -\eta_{137} = -\eta_{148} = 0.166E(1 - \nu^2)^{-1}\alpha^3x_B^{0.5}$
$-\eta_{116} = \eta_{125} = -\eta_{138} = \eta_{147} = 0.577E(1 - \nu^2)^{-0.5}\alpha^2d_1^{-1}x_B^{1.5}$
$\eta_{211} = \eta_{222} = \eta_{233} = \eta_{244} = 1.52E(1 - \nu^2)^{-0.25}\alpha^{1.5}d_1^{-1.5}x_B$
$\eta_{216} = -\eta_{225} = \eta_{238} = -\eta_{247} = -0.577E(1 - \nu^2)^{-0.5}\alpha^2d_1^{-1}x_B^{0.5}$
$-\eta_{311} = -\eta_{322} = -\eta_{333} = -\eta_{344} = 1.414x_A^{-0.5}$
$\eta_{312} = -\eta_{321} = \eta_{334} = -\eta_{343} = 0.76(1 - \nu^2)^{-0.25}\alpha^{0.5}d_1^{0.5}x_A^{-1}$
$\eta_{315} = \eta_{326} = \eta_{337} = \eta_{348} = -0.288(1 - \nu^2)^{-0.5}\alpha d_1 x_A^{-1.5} + x_A^{-0.5}$
$-\eta_{316} = \eta_{325} = -\eta_{338} = \eta_{347} = 0.537(1 - \nu^2)^{-0.25}\alpha^{0.5}d_1^{0.5}x_A^{-1} + x_A^{-0.5}$
$-\eta_{411} = -\eta_{422} = -\eta_{433} = -\eta_{444} = 2.632(1 - \nu^2)^{0.25}\alpha^{-0.5}d_1^{-0.5}x_A^{-1}$
$\eta_{412} = -\eta_{421} = \eta_{434} = \eta_{443} = 2.632(1 - \nu^2)^{0.25}\alpha^{-0.5}d_1^{-0.5}x_A^{-1} + 2.828x_A^{-1.5}$
$-\eta_{415} = -\eta_{426} = -\eta_{437} = -\eta_{448} = 1.074(1 - \nu^2)^{-0.25}\alpha^{0.5}d_1^{0.5}x_A^{-2} + x_A^{-1.5}$
$-\eta_{416} = \eta_{425} = -\eta_{438} = \eta_{447} = 3.722(1 - \nu^2)^{0.25}\alpha^{-0.5}d_1^{-0.5}x_A^{-1} + x_A^{-1.5}$

bending moment M_{B0} can be only calculated knowing the loosening coefficient of the joint. That is why the precise value of loosening coefficient can be only obtained through several steps. The solution starts with selecting the required residual gasket load under pressurized condition $F_{TU} > F_{T\min}$. Then using Eq. (12) the shearing force Q_{BU} and bending moment M_{BU} should be determined as the Fig. 5.b shows. Further on choosing arbitrarily starting values for M_{B0} and Q_{B0} with the help of Eqs. (8) and (10) the first approximation of the loosening coefficient can be obtained. Using the first approximating value of the loosening coefficient the values of M_{B0} and Q_{B0} with Eqs. (11) can be determined. Repeatedly substituting them into Eqs. (8) and (10) the next approximation for loosening coefficient can be gained. Following this method, in several steps the precise value of loosening coefficient can be obtained. The convergence of the method is testified by a numerical example in Chapter 5.

4. Stress-state of the Integrated Part

Knowing the loads on flange ring, the stress-state of the integrated part can be determined. At first the internal system of edge forces and moments acting on \overline{AB} calculating surface should be determined (see *Fig. 5*). In order to specify the actual stresses both on internal and external surfaces of the integrated part the system of loads described above should be reduced on $\overline{AB'}$ bisecting surface as it is shown in *Fig. 5*. This method permits the reduction mistake [8] originating from asymmetry of integrated part so the equations giving the stress-state of the flange [1, 4] can be made more precise. Following the above way of thinking the stress-state of the integrated part can be determined under seating *Eqs. (21)* and pressurized conditions *Eq. (22)*. The results are as follows:

$$\sigma_{1RK0} = \frac{6M_{1R0}}{\alpha^2 x^2} \sqrt{1 + \alpha^2}, \quad (21.a)$$

$$\sigma_{1RB0} = -\frac{6M_{1R0}}{\alpha^2 x^2}, \quad (21.b)$$

$$\sigma_{2R_B^K0} = \left(\frac{N_{2R0}}{\alpha x} \pm \nu \frac{6M_{1R0}}{\alpha^2 x^2} \right), \quad (21.c)$$

$$\sigma_{1RKU} = \left(\frac{6M_{1RU}}{\alpha^2 x^2} + p \frac{(d_1 - \alpha x_A)^2}{4[d_1 + \alpha(x - x_A)]\alpha x} \right) \sqrt{1 + \alpha^2}, \quad (22.a)$$

$$\sigma_{1RBU} = \left(-\frac{6M_{1RU}}{\alpha^2 x^2} + p \frac{(d_1 - \alpha x_A)^2}{4[d_1 + \alpha(x - x_A)]\alpha x} \right), \quad (22.b)$$

$$\sigma_{2R_B^KU} = \left(\frac{N_{2RU}}{\alpha x} \pm \nu \frac{6M_{1RU}}{\alpha^2 x^2} \right), \quad (22.c)$$

where in accordance with the symbols used in *Fig. 5* $\sigma_{1RK0}, \sigma_{1RB0}, \sigma_{2R_B^K0}, \sigma_{1RK\bar{U}}, \sigma_{1RBU}, \sigma_{2R_B^KU}$ mean the stresses under seating (0) and pressurized (U) conditions on the external (K) and internal (B) surfaces of the integrated part in the longitudinal (1) and circumferential (2) directions. The longitudinal edge moments M_{1R0}, M_{1RU} and the circumferential edge forces N_{2R0}, N_{2RU} acting on $\overline{AB'}$ bisecting surface of the integrated part can be

expressed in the following way:

$$M_{1R0} = \frac{M_{B0}\xi_{MB} + Q_{B0}\xi_{QB}}{d_1 + \alpha(x - x_A)}, \tag{23}$$

$$M_{1RU} = \frac{M_{BU}\xi_{MB} + Q_{BU}\xi_{QB} + p(\xi_P - g_5(x) - g_4)}{d_1 + \alpha(x - x_A)}, \tag{24}$$

where

$$\xi_\beta = g_1[\bar{c}_{(2i+2)\beta}\psi'_{(2i+1)}(\tilde{x}) - \bar{c}_{(2i+1)\beta}\psi'_{(2i+2)}(\tilde{x})]x^{1.5} + g_2[\bar{c}_{(2i+1)\beta}\psi_{(2i+2)}(\tilde{x}) - \bar{c}_{(2i+2)\beta}\psi_{(2i+1)}(\tilde{x})]x - g_3(\bar{c}_{j\beta}\psi'_j(\tilde{x}))x^{0.5}. \tag{25}$$

In *Eqs.* (24) and (25) the meaning of symbols applied are:

$$g_1 = 0.577E(1 - \nu^2)^{-0.5}\alpha^2, \tag{26.a}$$

$$g_2 = 0.438E(1 - \nu^2)^{-0.75}\alpha^{2.5}d_1^{0.5}, \tag{26.b}$$

$$g_3 = 0.166E(1 - \nu^2)^{-1}\alpha^3d_1, \tag{26.c}$$

$$g_4 = 0.02(2 - \nu)(1 - \nu^2)^{-1}\alpha^2d_1^3, \tag{26.d}$$

$$g_5 = 0.125\alpha(d_1 - \alpha x_A)^2(x - x_A). \tag{26.e}$$

$i = (0, 1)$, $j = (1, \dots, 4)$, $\beta = (MB, QB, P)$ further

$$N_{2R0} = \frac{2E\alpha x^{0.5}[M_{B0}\delta_{MB} + Q_{B0}\delta_{QB}]}{d_1 + \alpha(x - x_A)}, \tag{27}$$

$$N_{2RU} = \frac{2E\alpha x^{0.5}[M_{BU}\delta_{MB} + Q_{BU}\delta_{QB} + p\delta_P]}{d_1 + \alpha(x - x_A)} + 0.5p(d_1 + \alpha(x - x_A)), \tag{28}$$

where

$$\delta_\beta = \bar{c}_{j\beta}\psi'_j(\tilde{x}), \tag{29}$$

$j = (1, \dots, 4)$, $\beta = (MB, QB, P)$.

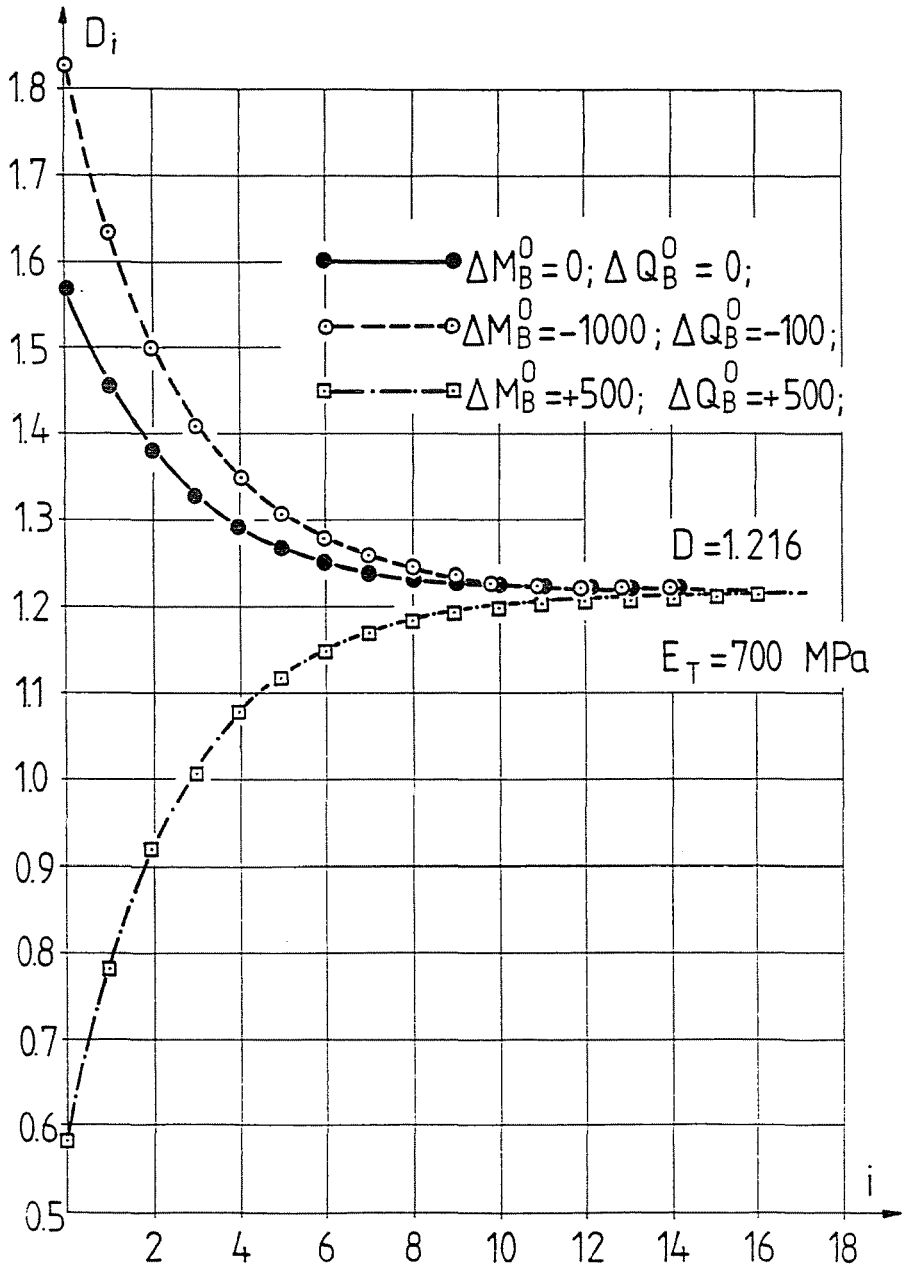


Fig. 7. The absolute convergence of the loosening coefficient during the trial-and-error calculations

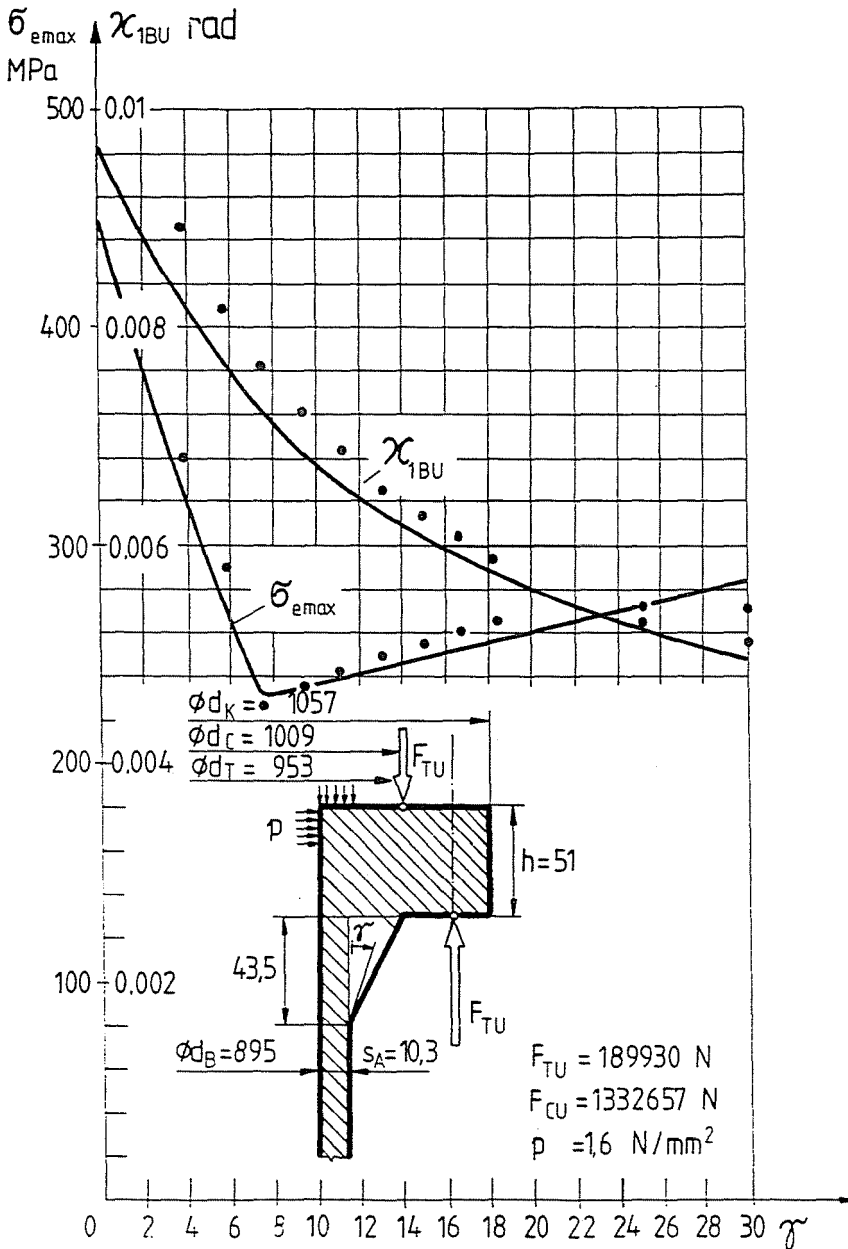


Fig. 8. The angular displacement of the flange ring and the maximum values of Mises stress in the integrated part as a function of cone-angle

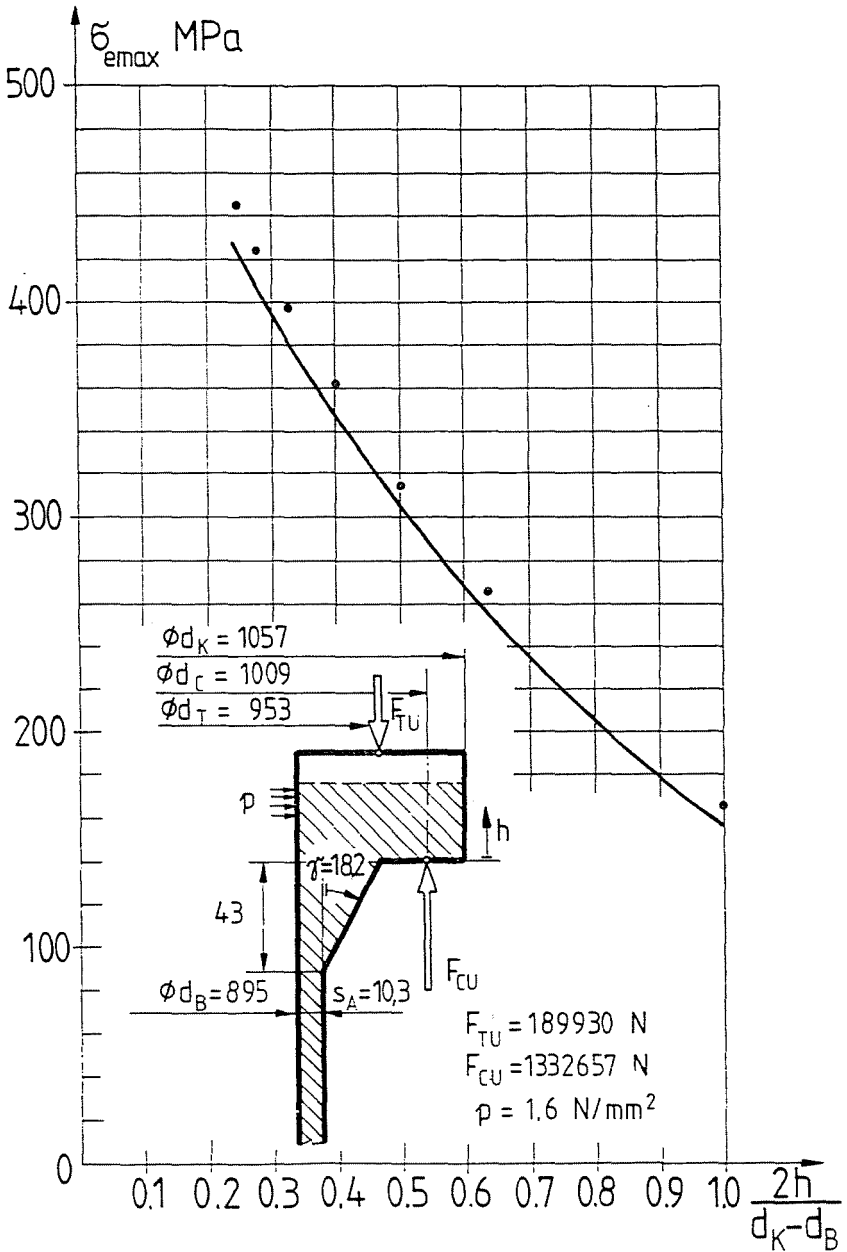


Fig. 9. The maximum values of Mises stress in the integrated part as a function of flange ring thickness

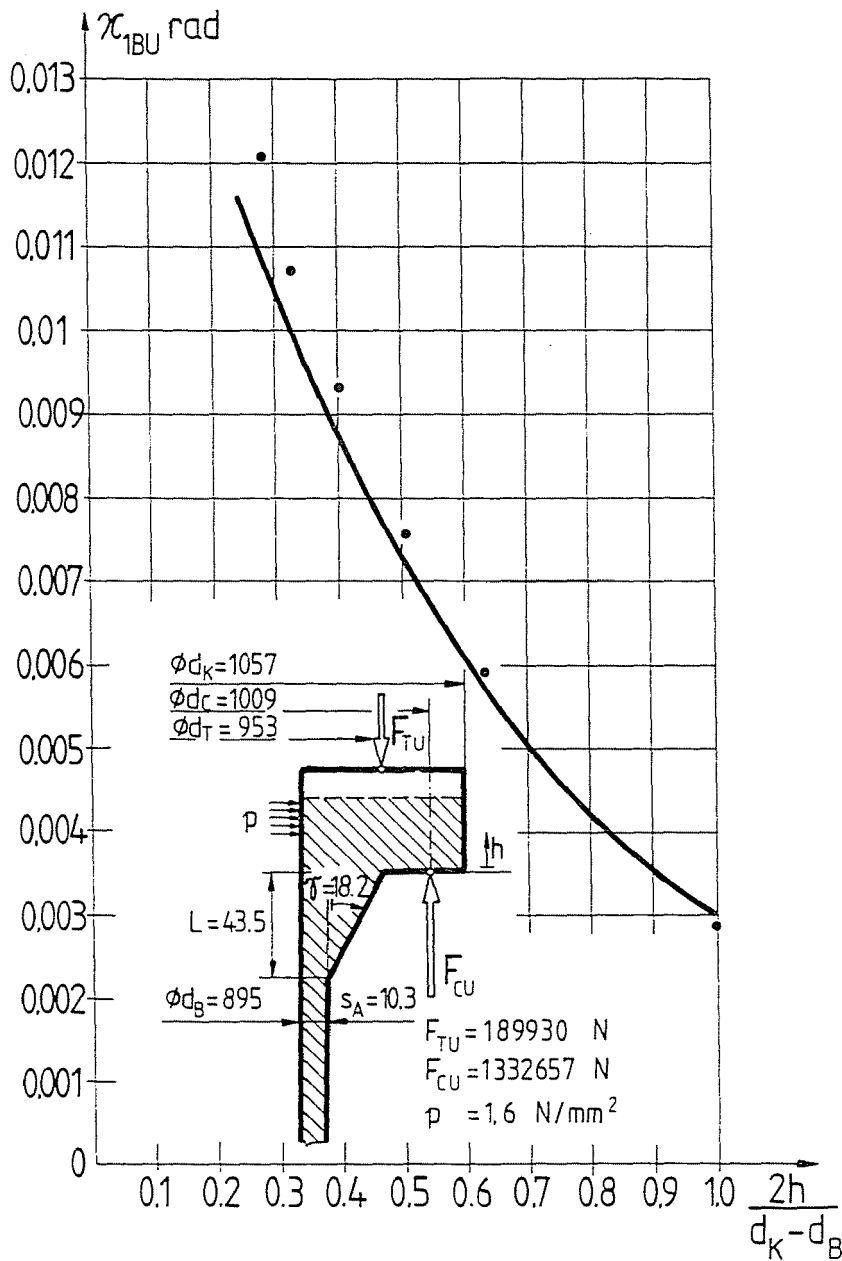


Fig. 10. The angular displacement of the flange ring as a function of its thickness

5. Numerical Example

The aim of this numerical example is to represent how to use the calculation method shown in Chapters 3 and 4 and to prove in practice the convergence of the applied trial-and-error method. The calculations presented here refer to a flange joint like the one with dimensions: $d_K = 1057$ (mm), $d_C = 1009$ (mm), $d_T = 953$ (mm), $d_B = 895$ (mm), $s_B = 24.6$ (mm), $s_A = 10.3$ (mm), $h = 51$ (mm), $L = 43.5$ (mm) seen in *Fig. 1*. To produce seating condition at the investigated flange joint there were $n = 44$ pcs. bolts with nominal diameter $d_0 = 18.9$ (mm) having the resultant spring stiffness $K_C = 4.05 \cdot 10^{-8}$ ($\frac{\text{mm}}{\text{N}}$). The sizes of the gasket producing leak-tightness were $b_T = 15.8$ (mm), $h_T = 3$ (mm), $d_T = 953$ (mm). During the calculations the value of operational pressure was $p = 1.6$ (MPa) and the required residual gasket load was $F_{TV} = 189930$ (N). Assuming ideal elastic gasket material model the loosening coefficient of the flange joint was determined. The compression spring stiffness of the gasket was regarded as a constant that is using the elasticity modulus $E_T = 700$ (MPa), $K_T = 9.06 \cdot 10^{-8}$ ($\frac{\text{mm}}{\text{N}}$) was obtained. The loosening coefficient of the joint was determined by the trial-and-error method shown in Chapter 3. To prove the convergence of this calculation method in practice in *Fig. 7* it is presented that the loosening coefficient trends to the same final value ($D = 1.216$) independent of the arbitrarily chosen initial values of ΔM_B^0 and ΔQ_B^0 . Finally, the preciseness of the equations referring to the rotational stiffness of the welding neck flange and the stress-state of the integrated part are proved by *Figs. 8, 9* and *10*. These figures represent the results of the finite-element investigations used as a control test. In these figures the angular displacement of the flange ring and the maximum value of Mises stress in the integrated part can be seen at pressurized condition as a function of cone-angle (*Fig. 8*) and the thickness of flange ring (*Fig. 9* and *10*). In these figures the continuous curves show the results of analytical, while points represent the values of finite-element calculations.

6. Conclusions and Possible Directions to Improve this Model

The numerical results shown in Chapter 5 clearly prove the convergence of the applied trial-and-error method and applicability of the model. The method worked out for calculation is applicable at different constructions of flange joint if its dimensions make possible to regard flange ring as an elastic ring and the effect of the integrated part can be determined as internal edge forces and moments by analytical equations. The characteristics of the

gaskets widely used in engineering practice are the non-linearity, the creep and stress relaxation under long-lasting static loads significant mainly at high operational temperatures. Therefore, as a further improvement of the calculation method published, the possibility of considering non-linearity, creep and stress relaxation of the gasket when determining the loosening coefficient should be found. This improvement would allow the use of this model at joints operating at high temperature.

References

1. WATERS, E. O. - WESSTROM, D. B. - ROSSHEIM, D. B. - WILLIAMS, F. S. G. (1937): Formulas for Stresses in Bolted Flanges Connections. *Trans of the ASME*, FSP-59-4, pp. 161-169.
2. LAKE, G.F - BOYD, G. (1957): Design of Bolted Flanged Joints of Pressure Vessels. *Proc. Inst. Mech. E.* Vol. 171, pp. 843-856.
3. TIMOSHENKO, S. - WOINOWSKI-KRIEGER, S. (1959): Theory of Plates and Shells. McGraw-Hill, New-York.
4. MURRAY, N. W. - STUART, D. G. (1961): Behaviour of Large Taper Hub Flanges. *Proc. Symp. Pressure Vessels Research Towards Better Design, I. Mech. E.* p. 133.
5. BERNHARD, H. J. (1963): Flange Theory and the Revised Standard B.S.10: 1962 - Flanges and Bolting for Pipes, Valves and Fittings. *Proc. Int. Mech. E.* Vol. 178, pp. 107-131.
6. VARGA, L. (1981): Untersuchung von Flanschkonstruktionen. *Konstruktion.* Vol. 33, pp. 361-365.
7. SINGH, K. P. - SOLLER, A. I. (1984): Mechanical Design of Heat Exchangers and Pressure Vessel Components. Arcturus Publishers, Cherry Hill, New Jersey, p. 81.
8. NAGY, A. (1991) Stress State Investigation of Integral-type Flange Joint. Diss. T.U. Budapest.